Thermodynamics of strain-induced crystallization in filled natural rubber under uni- and biaxial loadings, Part I: Complete energetic characterization and crystallinity evaluation

V.N. Khiêm, Jean-Benoit Le Cam, Sylvain Charles, M. Itskov

Thermodynamics of strain-induced crystallization in filled natural rubber under uni- and biaxial loadings. Part I: complete energetic characterization and crystallinity evaluation.

V.N. Khiêm[a], J.-B. Le Cam[b,*], S. Charlès[b], M. Itskov[a]

[a] *Department of Continuum Mechanics, RWTH Aachen University, Eilfschornsteinstr. 18 , 52062 Aachen, Germany*

[b] *Institut de Physique UMR 6251 CNRS/Université de Rennes 1, Rennes, France*

Abstract

The present paper provides the first full thermo-mechanical characterization of a crystallizing filled natural rubber under uniaxial and biaxial loadings. During the mechanical tests, the temperature was measured by using infrared thermography and processed by means of the heat diffusion equation for determining the corresponding heat power density. The intrinsic dissipation due to viscosity and stress softening are evaluated under cyclic loading by the energy balance. Energy contributions to the hysteresis loop converted into heat and stored in the material are distinguished. The heat power density is also used to evaluate the strain-induced crystallinity. This analysis provides new results on the energetic behavior of filled natural rubber. Accordingly, crystallization takes place under high biaxiality levels, close to the equibiaxial loading condition, while multiaxiality influences the crystallization onset. These experimental results are used in the second part of the present paper for a physically based modeling of the complex behavior of filled natural rubbers.

Keywords: Strain-induced crystallization, filled natural rubber, multiaxial loadings, infrared thermography, heat source, digital image correlation.

*Corresponding author. Fax : (+33) 223 236 111
Email address: jean-benoit.lecam@univ-rennes1.fr (J.-B. Le Cam)

1. Introduction

Physical phenomena involved in the deformation of natural rubber are numerous and complex. Most of them are still the subject of scientific debate, this concerns in particular strain-induced crystallization (SIC). Adding fillers to the polymer matrix makes the deformation mechanisms even more complicated; it induces viscosity and stress softening, increases cavitation and strongly influences SIC. Several experimental techniques can be used to identify and investigate these mechanisms, typically X-ray diffraction (XRD) (Katz, 1925; Toki et al., 2000; Trabelsi et al., 2002), X-ray microtomography (Legorju-Jago, 2007) and dilatometry (Feuchter, 1925; Ramier et al., 2007) as well as mechanical tests such as stress relaxation and cyclic loadings. Nevertheless, each of these techniques provides only partial information. In this context, several unverified assumptions have been formulated. For example, the energy involved in the hysteresis loop is considered to be mainly due to intrinsic dissipation and would be therefore converted into heat. Information obtained with the XRD technique[1] cannot be easily linked with continuum quantities and many assumptions have to be made in attempting to model SIC. Furthermore, SIC is generally investigated under uniaxial loadings and very few studies address multiaxial deformation cases. Beurrot-Borgarino (2012) and Brüning (2014), in their respective PhD thesis, reported XRD measurements with unfilled natural rubber specimens under equibiaxial loading. Here, they encountered a problem in reaching a sufficient stretch for crystallization. Typically, in the experiments by Beurrot-Borgarino (2012), the maximum displacement reached by the machine actuators was not enough. In the case of Brüning (2014), specimen failure occurred before applying the onset of crystallization. Further, Beurrot-Borgarino made similar experiments with a natural rubber filled with 50 phr[2] of carbon black, in order to reinforce the material and to expedite the crystallization onset. The author tested the filled natural rubber under uniaxial, biaxial and equibiaxial loadings and found similar crystallites under

[1] on the crystalline phase structure (Bunn, 1942; Takahashi and Kumano, 2004; Immirzi et al., 2005; Rajkumar et al., 2006), chain orientation (Toki et al., 2004), kinetics of crystallization (Toki et al., 2000; Trabelsi et al., 2003)

[2] part per hundred of rubber in weight)

uniaxial and equibiaxial tension: their size is of the same order of magnitude and the lattice parameters are identical. Under equibiaxial tension, the crystallinity index was equal to 1.09 % at a stretch of 4. Since then, only one recent study has investigated the effects of multiaxial loadings in crystallizing unfilled natural rubber with the XRD technique (Chen et al., 2019). The authors found that increasing the biaxiality level frustrates SIC. More specifically, no crystallization emerges by increasing the biaxiality level up to a ratio of the principal stretches of 1.6. Nevertheless, they were able to reach neither high stretch levels nor higher biaxiality level, i.e. equibiaxiality. The question of the multiaxial effects on SIC is therefore still open and new characterization techniques could therefore be used to enrich the knowledge in this field.

Considering that mechanisms involved in the deformation process are either endo- or exothermal, the question of their thermal and calorimetric characterization clearly arises. Indeed, calorimetric measurements are classically performed for studying metallic materials: the pioneering work by Farren and Taylor (1925) and Taylor and Quinney (1934) date from the 1920's and enabled the authors to measure the latent energy remaining after cold working in a metal under quasi-static monotone loadings. Today, fraction of the anelastic deformation energy rate irreversibly converted into heat in metals is studied through the Taylor-Quinney ratio by Chrysochoos (1985); Chrysochoos et al. (1989); Mason et al. (1994); Rittel (1999); Oliferuk et al. (2004). Polymer research has considerably benefited from this approach (see, e.g. Rittel (2000); Rittel and Rabin (2000); Benaarbia et al. (2014, 2015)). Despite the interest in such energetic characterization, papers on calorimetry under stretch applied to rubber are still scarce, while the first results have already provided important information on the thermo-mechanical behavior. For instance, it was shown that a hysteresis loop can form in the strain-stress relationship without any production of intrinsic dissipation, only due to SIC (Samaca Martinez et al., 2013b; Le Cam, 2017). Moreover, it was recently demonstrated that processing the calorimetric response provides an accurate evaluation of the crystallinity (Le Cam et al., 2020). In the case of non-crystallizing filled rubbers, fillers induce a hysteresis loop whose area does not entirely correspond to the energy converted into heat, as a certain amount of the mechanical energy is stored in the material.

This amount depends on the stretch and stretch rate level (Loukil et al., 2018).

This calorimetric technique has never been applied to both filled and crystallizing rubbers while it could provide relevant information for modeling, typically by providing the intrinsic dissipation due to viscosity or stress softening and by distinguishing the part of the hysteresis energy converted into heat and that one stored in the material. Furthermore, applying surface calorimetry to multiaxial tests could be of interest for investigating SIC.

The objective of this study is, therefore, to provide a full mechanical, thermal and calorimetric characterization of a filled natural rubber under uni- and multiaxial loadings. We believe that such a complete characterization is essential for a physically based modeling of SIC.

This paper is organized as follows. Section 2 recalls the theoretical framework for quantitative surface calorimetry. Section 3 presents the basis of energy balance over loading cycles. Section 4 briefly describes of the methodology for evaluating the strain-induced crystallinity from the calorimetric response. Section 5 deals with the experimental setup including testing machine, optical and infrared cameras used. Section 6 presents the results obtained under uniaxial loading conditions in terms of the mechanical, thermal and calorimetric responses. A complete energy balance of the filled natural rubber is established. The strain-induced crystallinity and the crystallization onsets are also evaluated with a special attention to the biaxial test. Similarly to the uniaxial tests, a complete characterization in particular with respect to SIC is carried out.

2. Theoretical framework for quantitative surface calorimetry

Quantitative surface calorimetry (QSC) consists of determining the heat power density, also called heat source, from temperature field measurements and the heat diffusion equation. The temperature fields measured with an infrared (IR) camera at the flat surface of a specimen are bidimensional and the tridimensional formulation of the heat diffusion equation has therefore to be simplified accordingly. This requires certain specimen geometries, loading conditions and assumptions, which will be presented in the following.

2.1. Tridimensional heat diffusion equation

Considering that the constitutive state equations are derived from the Helmholtz free energy function and that heat conduction follows Fourier's law, the local heat diffusion equation writes in the reference (Lagrangian) configuration as follows (Balandraud and Le Cam, 2014):

$$\rho_0 C\dot{T} + \mathrm{Div}\mathbf{Q} - R = \underbrace{\mathcal{D}_{int} + T\frac{\partial \mathbf{P}}{\partial T} : \dot{\mathbf{F}} + T\sum_{\beta=1}^{m} \frac{\partial \boldsymbol{A}_{\boldsymbol{\beta}}}{\partial T} : \dot{\boldsymbol{\xi}}_{\boldsymbol{\beta}}}_{\hat{S}} \tag{1}$$

where

- ρ_0 is the density,
- C is the heat capacity,
- T is the absolute temperature,
- $\mathbf{Q}$ is the heat influx per unit reference area,
- R is the external heat source (radiation, for instance),
- $\mathcal{D}_{int}$ is the intrinsic dissipation (also named mechanical dissipation),
- $\mathbf{P}$ is the first Piola-Kirchhoff stress tensor (or nominal stress tensor),
- $\mathbf{F}$ is the deformation gradient tensor,
- $\hat{S} = \mathcal{D}_{int} + T\frac{\partial \mathbf{P}}{\partial T} : \dot{\mathbf{F}} + T\sum_{\beta=1}^{m} \frac{\partial \boldsymbol{A}_{\boldsymbol{\beta}}}{\partial T} : \dot{\boldsymbol{\xi}}_{\boldsymbol{\beta}}$ denotes the heat source,
- the superposed dot stands for the material time derivative.

Note that $\mathbf{Q} = -\boldsymbol{K}_{\mathbf{0}}\mathbf{C}^{-1}det\mathbf{F}\mathrm{Grad}\,T$, where $\boldsymbol{K}_{\mathbf{0}}$ is the thermal conductivity tensor and $\mathbf{C} = \mathbf{F}^T\mathbf{F}$ is the right Cauchy-Green tensor.

In the right member, the term $T\frac{\partial \mathbf{P}}{\partial T} : \dot{\mathbf{F}}$ is the heat sources due to the entropic (and possibly isentopic) coupling. The term $T\frac{\partial \boldsymbol{A}_{\boldsymbol{\beta}}}{\partial T} : \dot{\boldsymbol{\xi}}_{\boldsymbol{\beta}}$ corresponds to the other thermomechanical

couplings. $\boldsymbol{\xi_\beta}$ are the internal tensorial variables, while $\boldsymbol{A_\beta}$ denote the corresponding thermodynamic forces.

2.2. Simplification of the heat diffusion equation and heat source reconstruction

The temperature fields provided by IR thermography are bidimensional. The reconstruction of the heat source field from them requires therefore the formulation of a two-dimensional version of the heat diffusion equation. To this end, the following assumptions are made:

- The heat conduction is considered as isotropic (the thermal conductivity coefficient is denoted k_0 in the following),
- The material is incompressible,
- The temperature is considered as constant over the specimen thickness. Thus, Eq. (1) can be integrated over the thickness. This means that the specimen must be relatively thin and that the plane stress state can be generally assumed. This leads to the two-dimensional formulation of the heat diffusion equation as

$$\rho_0 C \left(\dot{T} + \frac{T - T_{amb}}{\tau_{2D}} \right) - \mathrm{Div}_{2D}(k_0 \mathbf{C}^{-1} \mathrm{Grad}_{2D}\, T) - R \; = \hat{S}, \tag{2}$$

  where T_{amb} is the ambient temperature.

  τ_{2D} is a time characterizing the heat exchanges along the thickness direction by convection with the air at the specimen surface.

- The external radiations R are assumed to remain constant during the deformation process. In this case, R can be removed from the heat diffusion equation by using the temperature variation $\theta(X, Y, t) = T(X, Y, t) - T_{ref}(X, Y)$ instead of the temperature itself. It should be noted that T_{ref} is the ambient temperature if it is constant over the test. In this case, Eq. (2) writes:

$$\rho_0 C \left(\dot{\theta} + \frac{\theta}{\tau_{2D}} \right) - \mathrm{Div}_{2D}(k_0 \mathbf{C}^{-1} \mathrm{Grad}_{2D}\, \theta) = \hat{S}. \tag{3}$$

In practice, for materials with low thermal diffusivity such as rubbers, the thermal gradient remains confined to the area close to the grips. Therefore, given that heat conduction is negligible in the specimen plane or that heat exchanges with the grips of the testing machine does not induce temperature gradient in the measurement zone, the two-dimensional heat diffusion equation can be simplified (Chrysochoos, 1995; Berthel et al., 2008) and corresponds to a "0D" formulation of the heat diffusion equation:[3]

$$\rho C \left(\dot{\theta} + \frac{\theta}{\tau}\right) = \hat{S}. \tag{4}$$

This equation applies for homogeneous heat source field. As elastomeric materials are generally assumed to be incompressible, $\rho_0 = \rho$. Furthermore, it is assumed that $\tau_{2D} = \tau$. τ can be characterized from a natural return to room temperature after a heating (or a cooling) for each testing configuration (machine used, environment, etc). Indeed, in this case $\theta = \theta_0 e^{\frac{-(t-t_0)}{\tau}}$. Either τ is determined at different increasing stretches, further details are provided in Ref. Samaca Martinez et al. (2013b), or the value of τ is obtained in the undeformed state and corrected according to its dependency on the stretch and the multiaxiality state as follows:

$$\tau = \tau(\lambda, B) = \tau_0 \lambda^{-B-1}, \tag{5}$$

where $B = \frac{ln\lambda_2}{ln\lambda_1}$ denotes the biaxiality ratio, defined as the ratio are the maximum and minimum principal stretches in the loading plane, respectively. Under equi-biaxial tension, pure shear, and uniaxial tension, B is equal to 1, 0 and -0.5, respectively.

Remark #1: Note that the higher the initial length, the higher the displacement of the grips in the air for a given strain rate. Therefore, forced convection effects can be induced and τ has to be readjusted accordingly. This can easily be done when no intrinsic dissipation is produced, by verifying that the corresponding adiabatic temperature at the beginning and

[3]The relevancy of this assumption for a given situation can be evaluated by calculating the Biot number B_i (Louche, 2009).

the end of the cycles is the same (see for instance Le Cam et al. (2020). In filled rubbers, intrinsic dissipation is not zero and this verification is not possible anymore. This is the reason why a symmetric loading with a temperature measurement in the zone with almost zero displacement have to be preferred.

Remark #2: Although the concentration and physical parameters of fillers do not directly appear in (4)*, they strongly influence ρ, C and τ and thus indirectly affect the heat source.*

3. Energy balance

Here, we draw the energy balance of the specimen in order to evaluate the different energy contributions to the hysteresis loop. Recently, several studies have shown that the energy involved in the hysteresis loop is not entirely converted into heat. A part of it can be used by the material to change its microstructure. For instance, Le Cam (2017) has shown that in unfilled natural rubbers, the hysteresis is due to SIC[4], more specifically it is due to the difference in kinetics of crystallization and melting. Furthermore, the contribution of fillers added to elastomers to the hysteresis loop is not systematically the preponderant one, since a resulting additional energy can be stored in the deformed filler network, such as for carbon black filled acrylonitrile-butadiene rubber in Loukil et al. (2018). Thus, determining the part of the mechanical energy stored in filled crystallizing natural rubbers due to SIC and the filler network is very important for constitutive modeling. In the following, continuum quantities required for such an energy balance are listed.

- The total strain energy density (per unit referential volume) W_{strain} is the energy supplied mechanically to the material during the loading and the unloading,

$$W_{strain}^{load} = \int_{loading} \pi \, d\lambda \text{ and } W_{strain}^{unload} = \int_{unloading} \pi \, d\lambda, \text{ respectively,} \tag{6}$$

  where π denotes the first Piola-Kirchhoff stress in the loading direction and λ is the corresponding stretch.

[4]It should be noted that in the case of unfilled natural rubber, the assumption that SIC is responsible for the hysteresis loop was firstly reported in Clark et al (1940).

- The mechanical energy involved in the hysteresis loop W_{hyst}^{cycle} and the energy rate P_{hyst}^{cycle} are determined as follows:

$$W_{hyst}^{cycle} = W_{strain}^{load} - W_{strain}^{unload}, \; P_{hyst}^{cycle} = \frac{W_{hyst}^{cycle}}{t_{cycle}}, \tag{7}$$

where t_{cycle} denotes the duration of the cycle.

- Integrating the heat source over time of each cycle gives the mean intrinsic dissipation $\tilde{\mathcal{D}}_{int}$:

$$\tilde{\mathcal{D}}_{int} = \frac{1}{t_{cycle}} \int_{cycle} \hat{S} \; dt. \tag{8}$$

We recall here that intrinsic dissipation is due to irreversible processes, such as cavitation, viscosity, or reorganization of the filler network.

- The difference between P_{hyst}^{cycle} and $\tilde{\mathcal{D}}_{int}$ represents the energy stored in each cycle as

$$P_{stored}^{cycle} = P_{hyst}^{cycle} - \tilde{\mathcal{D}}_{int}. \tag{9}$$

It should be noted that some of the phenomena that cause intrinsic dissipation can also contribute to energy storage, for example nano-cavitation that affects SIC (Zhang et al., 2013; Demassieux et al., 2019) or the reorganization of the filler network (Loukil et al., 2018).

- The stored energy ratio γ_{se} is defined as

$$\gamma_{se} = \frac{W_{stored}^{cycle}}{W_{hyst}^{cycle}} \tag{10}$$

and further characterizes the ability of the material to store energy.

  - If γ_{se} tends to 0, no energy is stored during the deformation. The whole hysteresis loop is due to the intrinsic dissipation.

- If γ_{se} tends to 1, the whole hysteresis loop is due to stored energy and no intrinsic dissipation is detected. This is typically the case in unfilled natural rubber (Samaca Martinez et al., 2013b).

It should be noted that this ratio can be influenced by both the strain range and the strain rate applied to the specimen (Lachhab et al., 2018).

4. Strain-induced crystallinity evaluation

As mentioned earlier, the strain-induced crystallinity of rubber is classically evaluated by XRD. In addition, XRD provides important information on the crystalline phase structure (Bunn, 1942; Takahashi and Kumano, 2004; Immirzi et al., 2005; Rajkumar et al., 2006), chain orientation (Toki et al., 2004), kinetics of crystallization (Toki et al., 2000; Trabelsi et al., 2003). SIC is an exothermal process so that alternative methodologies based on temperature or calorimetry measurements can be applied to determine the crystallinity. For instance, Le Cam (2018) proposed a technique for evaluating this thermal energy and the corresponding temperature variation due to SIC (denoted ΔT_{cryst}). The crystallinity is obtained by assuming that the crystallization energy of natural rubber can be approximated by the enthalpy of fusion ΔH_{cryst} assumed to be independent of temperature and stretch. Here, as a first approach, we use the value determined by Roberts and Mandelkern (1955), and set $\Delta H_{cryst} = 59,9\ J.cm^{-3}$. The crystallinity can be expressed in terms of ΔT_{cryst} as follows:

$$\zeta(t) = \frac{\rho C \Delta T_{cryst}(t)}{\Delta H_{cryst}}. \tag{11}$$

Results obtained with this method show very good agreement with those obtained with the XRD technique when applied to the same unfilled natural rubber (Le Cam et al., 2020). For filled materials, this ratio was weighted by a factor $\frac{1}{1-\Phi_{filler}}$, where Φ is the filler volume fraction. Moreover, the prediction of the heat source without crystallization accounts for both the elastic coupling and the intrinsic dissipation.

5. Experimental set-up

5.1. Material

The material considered in the present study is a natural rubber (*cis*-1,4 polyisoprene) provided by the Contitech AVS France company. It is vulcanised with sulphur and filled with carbon black aggregates. Table 1 summarizes its chemical composition. Values of the

Ingredients	Quantity (phr)
NR	100
Zinc oxide	10
Plastificant	< 3
Carbon black	20-30
Sulphur	1.5
Stearic acid	2
Antioxidant	2-4
Accelerators	2-4

Table 1: Chemical composition of the natural rubber

density ρ, the heat capacity C and the thermal conductivity k_0 are issued from the literature and are equal respectively to 0.94 kg/dm^3, 1750 $J/(kg.K)$ and 0.2 $W/(m.K)$.

5.2. Loading conditions and specimen geometries

Two types of tests were carried out with different specimen geometries: uniaxial tension of a dumbbell-like specimen and biaxial tension of a cruciform specimen. The latter leads to heterogeneous strain/stress fields, allowing to investigate multiaxial effects on both the thermomechanical response and SIC.

5.2.1. Uniaxial loading conditions

Uniaxial tensile tests were performed with a 24 mm long, 10 mm wide and 2 mm thick specimen, with cylindrical branch ends to avoid any slippage in the machine grips, as depicted in Figure 1. This geometry leads to a homogeneous uniaxial strain/stress state in the entire specimen except in the zones close to the grips (see the specimen geometry).

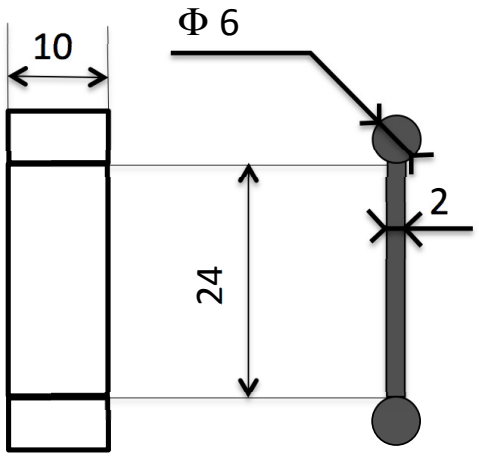

Figure 1: Specimen geometry for the uniaxial homogeneous tests (dimensions in mm)

Four types of uniaxial tensile tests (#1 to #3*b*) were carried out kinematically controlled at the velocity of 300 mm/min. Stretch profiles of the tests are shown in Figure 2. The loading was applied symmetrically with the two vertical actuators of the biaxial testing machine being shown in Figure 3 and described in the next paragraph. In Test #1, 3 cycles at increasing maximum stretch levels; 2.5, 4 and 6 were applied. This test allows for characterizing the typical phenomena involved in the mechanical response as the hysteresis loop, the permanent set, the accommodation, also referred to as the Mullins effect in the literature (Mullins, 1948), and the stress hardening at large strains.

In order to better investigate the time dependency of the mechanical response due to both the viscosity induced by fillers and SIC, Test #2 included relaxation phases of 60 s in the stretch profile of Test #1:

- at the end of the last loading of each set,
- during the last final unloading at decreasing stretches equal to 6, 4 and 2.5.

Test #3*b* corresponded to Test #2 but the material was preconditioned during Test #3*a* in order to remove the Mullins effect observed in the mechanical response of Test #2. Note that in contrast to the most of previous studies with the preconditioning, the permanent set

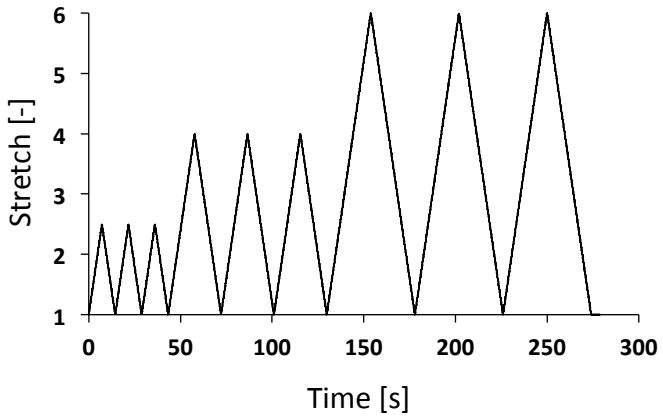

(a) *Test #1: without relaxation phases*

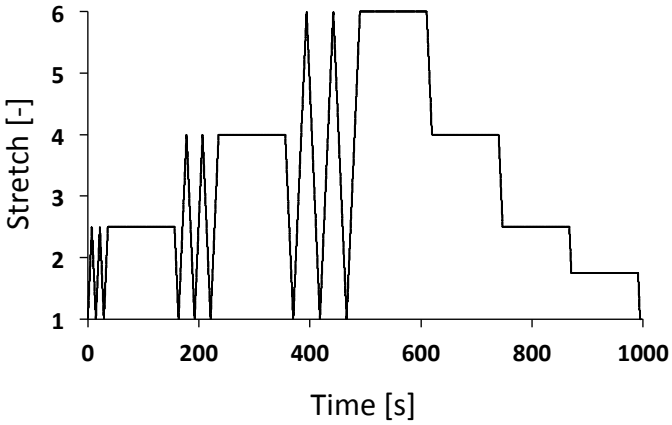

(b) *Tests #2 and #3b: with relaxation phases*

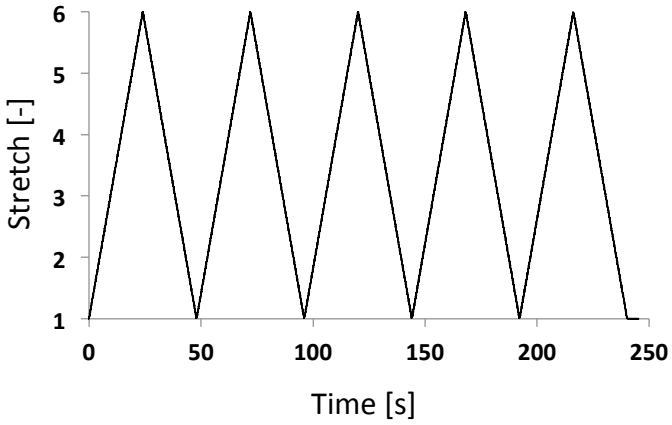

(c) *Test #3a: preconditioning phases*

Figure 2: Stretch-time curves for the four uniaxial tensile tests performed at 300 mm/min

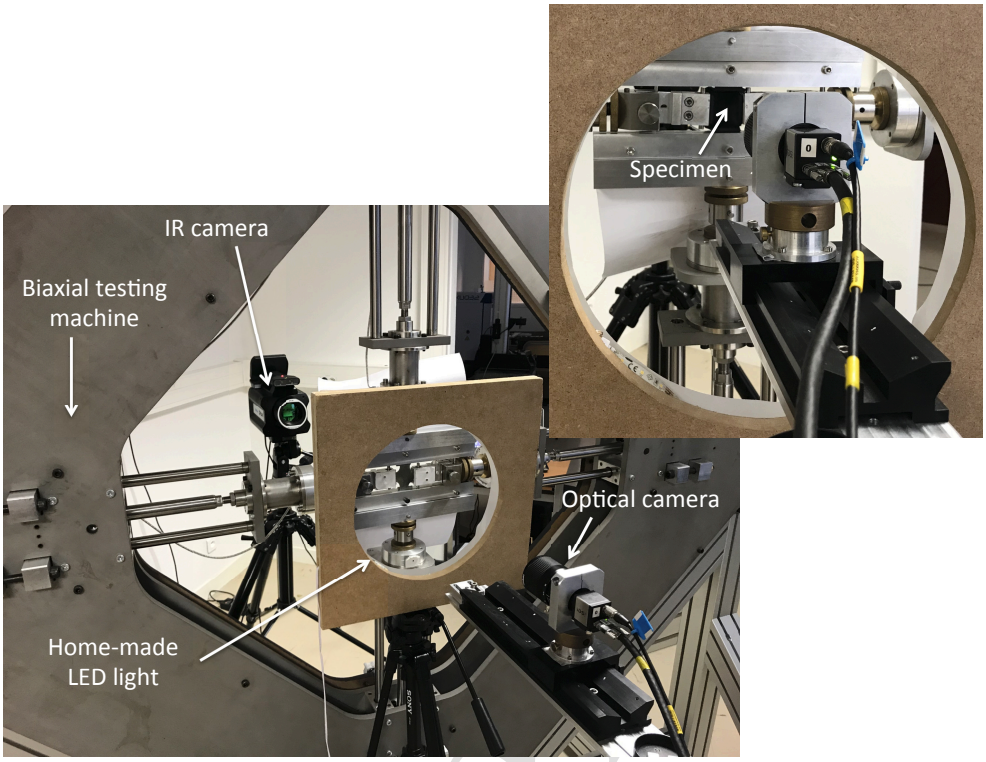

Figure 3: Overview of the experimental setup

observed after Test #3a was further taken into account. For Test #3b, the stretch imposed has been calculated by considering the same initial length as for Test #3a. All the tests were performed at $21 \pm 1°C$.

5.2.2. Biaxial loading conditions

Multiaxial loading effects were investigated in a biaxial test with a cross-shaped specimen. The specimen extremities were wrapped around a metallic roll. The initial lengths in the horizontal and vertical directions are slightly different as 39.5 and 49.5 mm, respectively. The specimen geometry is shown in Figure 4.

Figure 3 presents an overview of the experimental setup, which comprises a home-made biaxial testing machine with four independent electrical actuators controlled by an in-house LabVIEW program and two cameras (infrared (IR) and optical) placed on both sides of the

specimen. The four specimen branch ends were displaced up to 150 mm at a rate of 150 mm/min (see Figure 5).

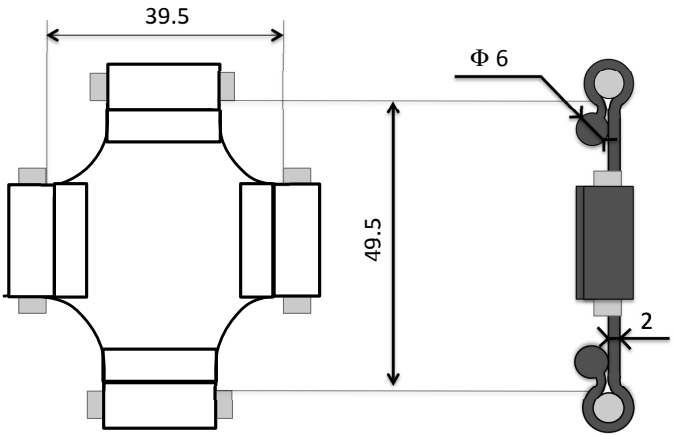

Figure 4: Specimen geometry for the biaxial test (dimensions in mm)

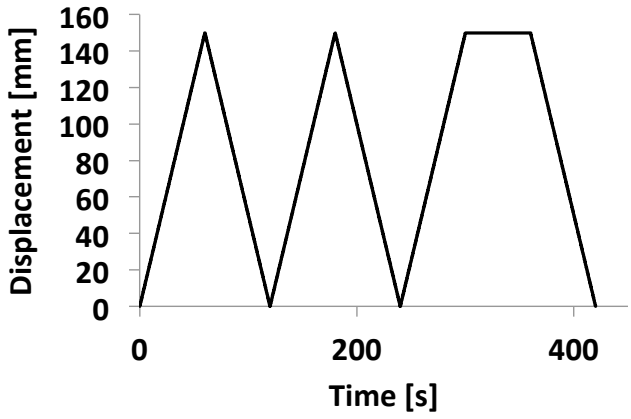

Figure 5: Profile of the mechanical loading applied for the biaxial tensile test

5.3. Full kinematic field measurement

In order to characterize the strain state at the center of the cruciform specimen during the biaxial test, 5 images per second were stored by a IDS camera equipped with a 55 mm telecentric objective. The charge-coupled device (CCD) of the camera has 1,920 × 1,200

joined pixels. The displacement and strain fields were determined by the digital image correlation (DIC) technique. The software used for the correlation process was SeptD (Vacher et al., 1999). To this end, a white paint was sprayed on the surface of the specimen before testing. A suitable contrast in terms of grey level is ensured at the specimen surface with a home-made LED lamp (Fig. 3), which provides a uniform cold lighting. In this configuration, a Region Of Interest (ROI) of 500 $\times$ 700 px is observed by the digital camera in the undeformed state. The spatial resolution was equal to 35.8 $\mu m/px$. Due to large displacement of the points during the test, the ROI was reduced to 320 $\times$ 340 px. The displacement was determined with a ZOI of 20 $\times$ 20 px and a grid step of 20 px. Therefore, the spatial resolution of the displacement field, defined as the smallest distance between two independent points was 20 px, i.e. 0.716 mm. This is sufficient considering that in the observed zone strain gradients are relatively small for such specimen geometry.

5.4. Full thermal field measurement

Temperature measurements were performed by using a cooled FLIR IR camera equipped with a focal plane array of 640 $\times$ 512 pixels and detectors operating in wavelengths between 1.5 and 5.1 μm. The thermal and kinematic measurements were synchronized at 5 images per second. The integration time was 2623 μs. The calibration of camera detectors was performed with a black body using a one-point Non-Uniformity Correction (NUC) procedure at this acquisition frequency. The thermal resolution or noise equivalent temperature difference (NETD) is 20 mK for a temperature range between 5 and 40°C. The spatial resolution of the thermal field was 212 μm/px. The IR camera was switched on several hours before testing in order to stabilize its internal temperature. The surface emissivity of the material was evaluated by comparing the temperature of the specimen surface placed in an oven and heated to 50°C with the one of a black body regulated at the same temperature. The emissivity of 0.94 was obtained. In uniaxial tests, the temperature is averaged in the central zone of the specimen with almost zero displacement. The size of the zone has no significant effect on the temperature measurement since the temperature variation to be quantified has the order of magnitude of several K while the thermal resolution is equal to

20 mK and the temperature field is homogeneous in this zone.

6. Results

6.1. Uniaxial tensile tests

In this section, the mechanical response measured in the four tests is first discussed. Then, the corresponding temperature variation and heat source are characterized. From the heat source, the intrinsic dissipation due to viscosity and stress softening as well as the relative part of the hysteresis loop corresponding to the energy stored in the material (see Sections 2 and 3) are determined. The strain-induced crystallinity is finally evaluated by using the methodology described in Section 4.

6.1.1. Mechanical responses

Results of Test #1 are shown in Fig. 6(a). The classical mechanical response of a filled rubber under cyclic loadings characterized by non-linear elasticity, large strains, hysteresis loop and the well-known accommodation first highlighted by Bouasse and Carrière (1903) and deeply investigated by Mullins and co-workers from the 1940s (Mullins, 1948) can be seen here. Note that the accommodation level is significant even though the amount of fillers is inferior to 20 *phr*. This was previously highlighted by Harwood et al. (1965). Therefore, a low amount of fillers is sufficient to significantly activate the Mullins effect, but not the viscosity. The three other tests aim at characterizing both the accommodation and viscous effects. Fig. 6(b) shows the mechanical response during the specimen preconditioning (Test #3*a*). The material is loaded at a maximum stretch of 6 and the stabilized response is similar to that one obtained if cycles at lower maximum stretches are applied before (see Fig. 6(a), Test #1).

Including relaxation phases at the end of the last loads of each set of 3 cycles does not affect the stress-strain response of the following cycles (see Fig. 6(c)). The stress relaxation is mainly observed for the maximum stretch of 6. When the specimen is pre-conditioned (Test #3*b*, Fig. 2(d)), the Mullins effect no longer appears in the mechanical response. The

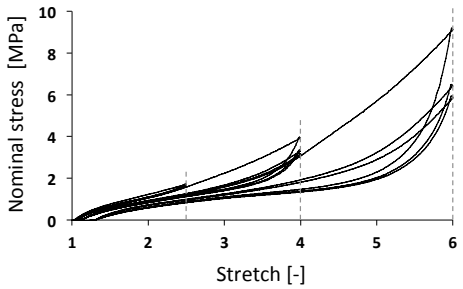

(a) *Test #1: without relaxation phases*

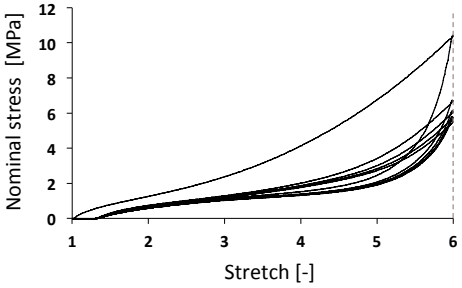

(b) *Test #3a: preconditioning phases*

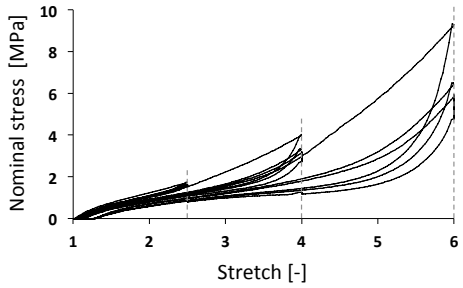

(c) *Test #2: with relaxation phases*

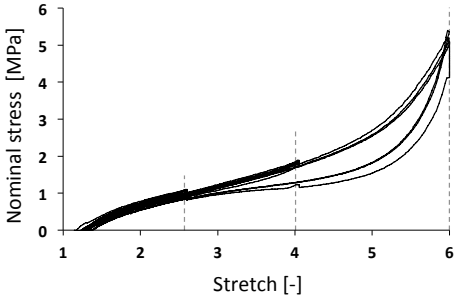

(d) *Test #3b: with relaxation phases after preconditioning*

Figure 6: Experimental stress-stretch curves

hysteresis loop can only be due to viscosity and SIC. According to diagram in Fig. 6(d), hysteresis increases much stronger at $\lambda = 6$ in comparison to $\lambda = 4$ than at $\lambda = 4$ in comparison to $\lambda = 2$. Since SIC starts slightly under $\lambda = 4$, we can conclude that this increase is mostly due to SIC. Furthermore, during the last unloading where three pauses were applied, viscous effects are very small. Indeed, in contrast to crystallization, melting is assumed to occur instantaneously. Thus, the only stress recovery effect should have been due to viscosity. As the relaxation is very low at $\lambda = 4$ (stretch close to the onset of SIC), the effect of viscosity on the relaxation should be low compared to that of SIC. These different conclusions cannot be definitely drawn solely on the basis of the mechanical response and further investigations are carried out with the calorimetric measurements.

6.1.2. Thermal responses

The thermal response measured during the different tests is illustrated in Figure 7. Rather weak self-heating of the material can be observed, which indicates that little intrinsic dissipation is produced at each cycle and therefore the viscous effect is low. This corresponds with the previous analysis (section 6.1.1). Furthermore, in contrast to unfilled natural rubbers (see Joule (1857); Anthony et al. (1942); Samaca Martinez et al. (2013a)), the thermoelastic inversion is not observed in the thermal response. [5] This is explained by the fact that the heat produced by the intrinsic dissipation is superior to the heat absorbed by the material at the very small stretches. Since the thermal response does not allow for quantifying neither the intrinsic dissipation nor the crystallinity under non-adiabatic conditions, a calorimetric analysis is required.

6.1.3. Calorimetric responses

Figure 8 presents calorimetric responses of Tests #1, #2, #3*a* and #3*b*, determined on the basis of the temperature measurements and the simplified heat diffusion equation (Eq. 4). First of all, no significant difference was observed between the first three cycles at $\lambda = 2$ in non preconditioned materials. Moreover, the heat source is relatively symmetrical between loading and unloading. A strong difference in the accommodation is obtained between the first and the following loadings. The area between them, which appears in color in the diagrams, corresponds to the energy dissipated due to the Mullins effect.

Furthermore, the heat sources for cycles at the maximum stretches of 4 and 6 were symmetrical. The occurrence of a dissymmetry when increasing the stretch is the typical calorimetric signature of SIC (see for instance Samaca Martinez et al. (2013b) or Lachhab et al. (2018)). During the stabilized loading cycles in Test #1, a strong increase in the slope of the heat source curve is observed when SIC starts. This increase is observed at stretch of 2.7 and 3.1 approximately for the loading cycles with the maximal stretch amplitude of 4 and 6, respectively. Test #3*a* led to the same result. This is due to the permanent set

[5] The thermoelastic inversion characterizes the fact that the temperature first decreases at the very low stretches, typically inferior to 7%, before increasing at higher stretches.

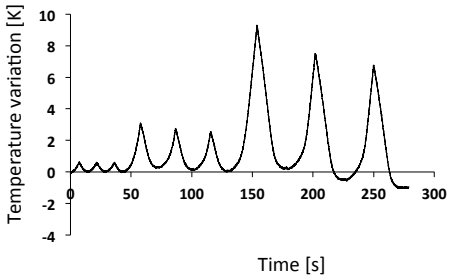

(a) *Test #1: without relaxation phases*

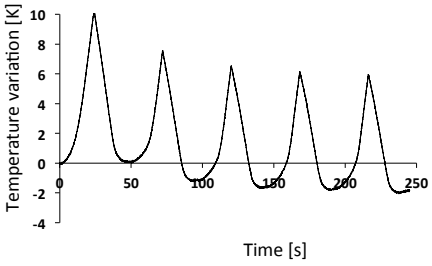

(b) *Test #3a: preconditioning phases*

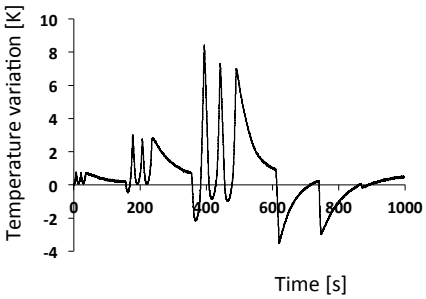

(c) *Test #2: with relaxation phases*

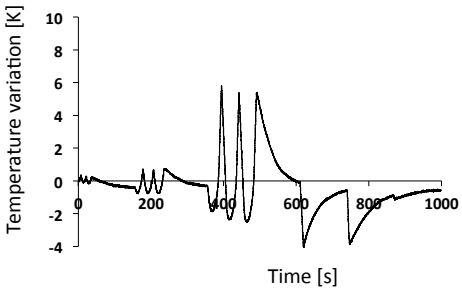

(d) *Test #3b: with relaxation phases after preconditioning*

Figure 7: Temperature variation versus stretch curves

effect that increases the initial length (14% and 30% for cycles at maximum stretches of 4 and 6, respectively). Therefore, the onset of SIC can be recalculated by accounting that the specimen was previously accommodated and has higher initial length. In this case, the onset of SIC return to a same stretch value, i.e. 2.4. Thus, the influence of the permanent set, preconditioning and the maximal cyclic stretch on the onset of SIC is very complex and should further be studied. This is why, the exact conditions used to evaluate this onset have to be clearly explained, which is not the case in many studies. For further SIC characterization, the crystallinity is evaluated versus stretch in Section 6.1.5.

For the tests with relaxation phases (Tests #2 and #3*b*), similar conclusions can be drawn. Nevertheless, focusing on the unloads, a strong heat absorption is observed after the pause at $\lambda = 4$ ((see arrows in Figs. 8(c) and (d))). Without this pause, this level of heat absorption could not be reached. The only explanation for this phenomenon is that the SIC is time

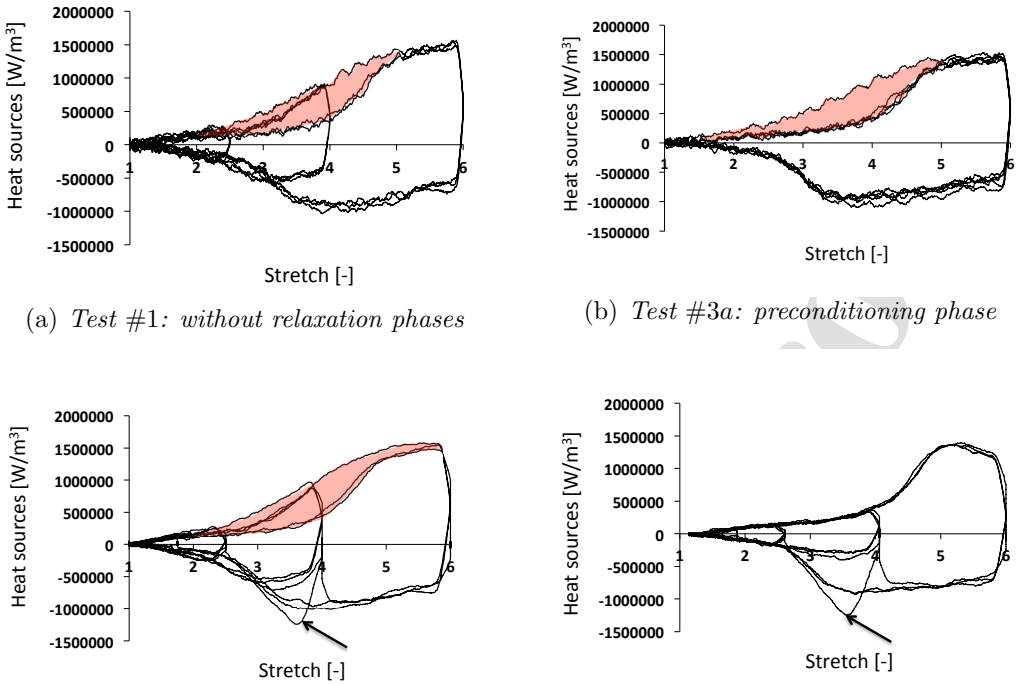

(a) *Test #1: without relaxation phases*

(b) *Test #3a: preconditioning phase*

(c) *Test #2: with relaxation phases*

(d) *Test #3b: with relaxation phases after preconditioning*

Figure 8: Heat source versus stretch curves

dependent process and the pause allows for the increase of crystallinity. Therefore, more energy is absorbed due to additional melting when the stretch decreases from 4. The fact that this effect was not observed at $\lambda = 6$ has to be further investigated with respect to the crystallite typology and the fact that the SIC kinetic rate increases when the maximum stretch applied increases (Huneau, 2011). This is an important experimental result for modeling SIC. It should finally be noted that after prestretch to $\lambda = 6$, the dissymmetry in the cycles is less important at $\lambda = 4$.

The mean intrinsic dissipation $\tilde{\mathcal{D}}_{int}$ can be obtained as a time integral of the heat sources over the cycle time, normalized by the cycle duration (see Eq. 8). Then, $\tilde{\mathcal{D}}_{int}$ was calculated for the third cycle of each stretch amplitude and is only due to viscosity. From Figure 9, we can observe that $\tilde{\mathcal{D}}_{int}$ evolves almost linearly with the stretch. This is important information for modeling the viscosity in filled natural rubber.

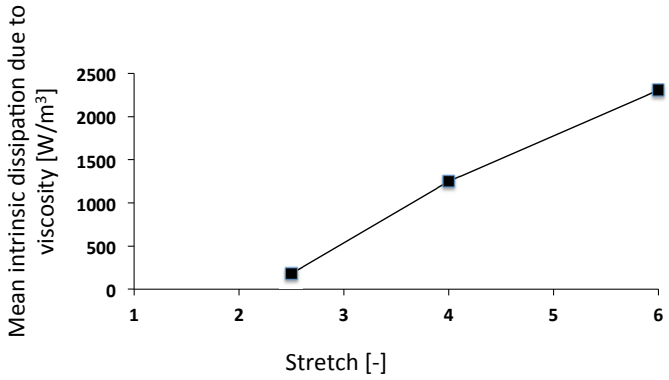

Figure 9: Mean intrinsic dissipation ($\tilde{\mathcal{D}}_{int}$) due to viscosity plotted versus stretch. $\tilde{\mathcal{D}}_{int}$ is evaluated from the mechanically and thermally stabilized cycles of Test #1

As the heat source curves obtained for the unloads were all superimposed in the tests without relaxation phases, the energy involved in the accommodation (Tests #1, #2 and #3*a*) can be approximated as the areas highlighted in red in Figs. 8(a), (b) and (c). Thus, the third cycles of each stretch amplitude are assumed to be fully accommodated. The mean intrinsic dissipation due to the accommodation (the calorimetric signature of the Mullins effect) is evaluated by subtracting the mean intrinsic dissipation obtained at the third from the first cycles (Samaca Martinez et al., 2014). Figure 9 illustrates the results obtained for Tests #1. From this figure, it becomes apparent that the mean intrinsic dissipation produced by the Mullins effect increases almost linearly with the stretch, but the slope is lower than the one of the intrinsic dissipation due to viscosity only. Indeed, the Mullins effect contributes to 81%, 64% and 58% to the mean intrinsic dissipation involved in the first cycles at the maximal stretches of 2.5, 4 and 6, respectively. This is the same order of magnitude as Samaca Martinez et al. (2014) found for a 50 phr carbon black filled natural rubber.

6.1.4. Energy balance

Energy balance is investigated in order to evaluate relative contributions of the physical phenomena involved in the hysteresis loop. Recently, it was shown that viscosity is not the only origin of the hysteresis loop. Indeed, energy stored and fully or partially released with

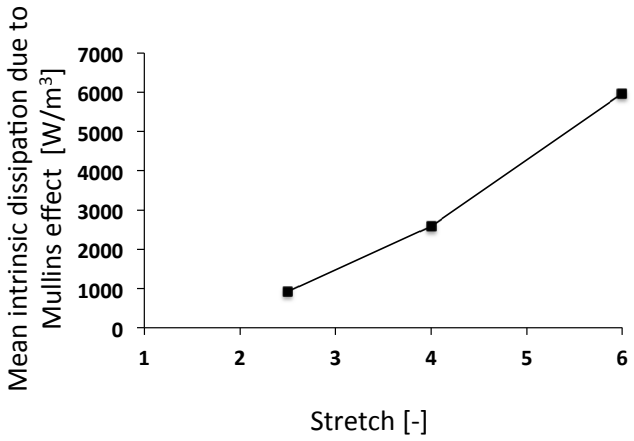

Figure 10: Mean intrinsic dissipation due to Mullins effect versus stretch evaluated from Test #1

a different rate also contributes to the hysteresis loop. This energy storage can be not only due to SIC (Le Cam, 2017; Lachhab et al., 2018), but also due to the filler network (Loukil et al., 2018). These studies clearly highlight that the hysteresis loop cannot be only due to phenomena that produces intrinsic dissipation such as viscosity or nano-cavitation. To quantify the relative contribution of the energy storage in rubbers, the γ_{se} ratio (10) has recently been introduced in Loukil et al. (2018) and is plotted versus stretch in Fig. 11. In Test #1, the viscosity is responsible for more than 80% ($\gamma_{se} < 0.2$) of hysteresis at a maximal stretch of 2 and 4. With higher stretches the contribution of viscosity reduces, while the energy storage increases up to 50% as a result of crystallinity. Obviously, such an effect is of an important benefit for limiting the self-heating and the energy available for damage, which explains the remarkable mechanical properties of filled natural rubbers.

6.1.5. Strain-induced crystallinity

The strain-induced crystallinity has been evaluated with the methodology described in Le Cam (2018) from the last cycle of Test #3*a*. In Figure 12, the heat source versus stretch is plotted. The heat source without crystallization is approximated by the following function:

$$\hat{s}_{predicted} = C_1(\lambda - \lambda^{-2B-3}) + C_2(\lambda - \lambda^{-2B-3})^2 + C_3(\lambda - \lambda^{-2B-3})^3. \quad (12)$$

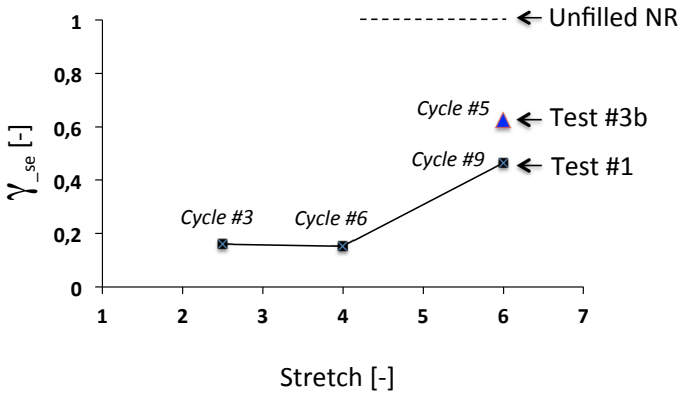

Figure 11: γ_{se} evaluated from thermodynamic cycles: cycles #3, #6 and #9 for Test #1 and cycle #5 for Test #3*b*. As indicated on the diagram, the value of γ_{se} is approximately 1 for unfilled natural rubbers.

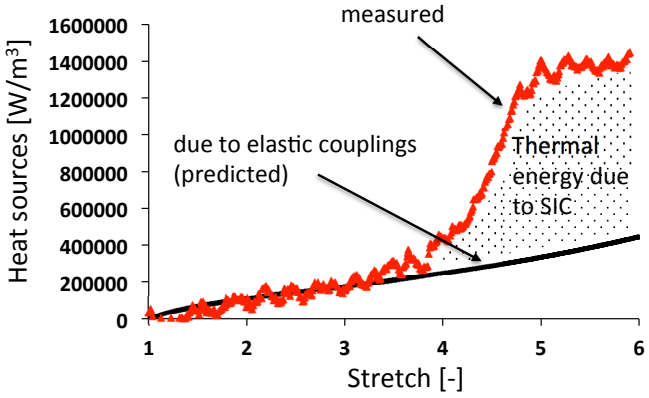

Figure 12: Evaluation of the thermal energy due to SIC for the 5^{th} cycle in Test #3*a*. The heat source measured and its predicted contribution only due to the elastic coupling are plotted in red and black, respectively.

The polynomial coefficients were identified by fitting the heat source curve before SIC starts, i.e. at $\lambda = 3.2$. The thermal energy due to SIC corresponds to the area between the two curves (see Fig. 12). The temperature variation due to SIC and the crystallinity is then calculated (for more details see Le Cam (2018)). In Fig. 13 the so resulting crystallinity is plotted versus stretch. The maximum value reaches 13.2%, which is in good agreement

with the measurement performed by using X-ray diffraction in Marchal (2006) in a natural rubber with a chemical composition (sulfur amount and filler amount) close to the present one.

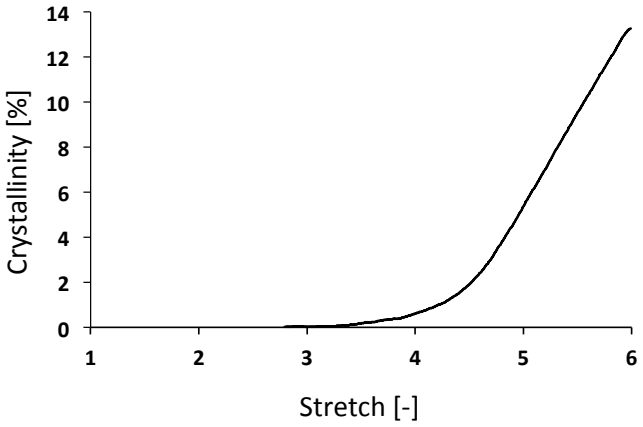

Figure 13: Prediction of the strain-induced crystallinity versus stretch

6.2. Biaxial tensile tests

This section aims to characterize the thermal and calorimetric responses of the filled natural rubber under a highly multiaxial strain state, i.e. under a high value of the biaxiality coefficient. The strain-induced crystallinity is also evaluated by the surface calorimetry technique presented in Section 4 and discussed in Beurrot-Borgarino (2012) and Chen et al. (2019).

Previously, SIC was mostly studied under uniaxial loadings. Rare studies investigated multiaxial effects on SIC, although the phenomenon appears to be strongly affected by the biaxiality of the strain state. In the case of unfilled natural rubber, an increase of the biaxiality coefficient from uniaxial tension was recently found in Chen et al. (2019) to suppress or strongly reduce SIC. Specifically, the authors found that no crystallization emerges even under large stretch levels up to specimen fracture. It should be noted that the maximum value of the biaxiality coefficient was equal to 0.6. In contrast, upon testing a filled natural

rubber under uniaxial, biaxial and equibiaxial loading conditions, Beurrot-Borgarino (2012) found similar crystallites under uniaxial and equibiaxial tension: their size was of the same order of magnitude and the lattice parameters were identical. Under equibiaxial tension with $\lambda = 4$, a crystallinity index was evaluated to 1.09 %. The methodology used to determine the crystallinity index is presented in Beurrot-Borgarino et al. (2014). Furthermore, even though the misorientation between uniaxial and planar tension was constant and small, it strongly increased with the biaxiality, in such a way that the crystallites did not demonstrate any preferred direction under equibiaxial loading. Thus, the question of how the loading multiaxiality affects SIC is under-explored and new characterization techniques, such as the one presented in this paper, appear indispensable to enrich the knowledge in this field.

6.2.1. Kinematics of the specimen center

The kinematics of the zone at the specimen center was investigated from the DIC measurements. In Figure 14 the principal stretches, the biaxiality coefficient in the specimen plane and the displacement imposed in each branch are plotted versus time. Gray strips indicate time intervals where buckling occurred. The maximal principal stretch exceeded 3 for the maximum displacement applied, which is very close to the stretch at which crystallization started under uniaxial tension. The value of the biaxiality coefficient varies between 0 (shear) and 1 (equibiaxial tension) during the cycles. Note that its value is superior to 0.8, which is close to the equibiaxial loading condition, for maximum principal stretches superior to 2.

6.2.2. Thermal and calorimetric response of the specimen center

In Figure 15 the temperature, the heat source and the displacement applied to each branch are plotted versus time. The heat source has been calculated by accounting for the change in the biaxiality ratio in the calculation of $\tau(\lambda, B)$ (see Eq 5). During the first loading, a strong heat production occurred due to the Mullins effect (Circles #1 and #2), so that it was not possible to distinguish the heat produced by the thermo-elastic couplings, the viscosity or crystallization from the heat produced by the Mullins effect. During the next cycle, a significant change in the curve slope was observed during the first loading,

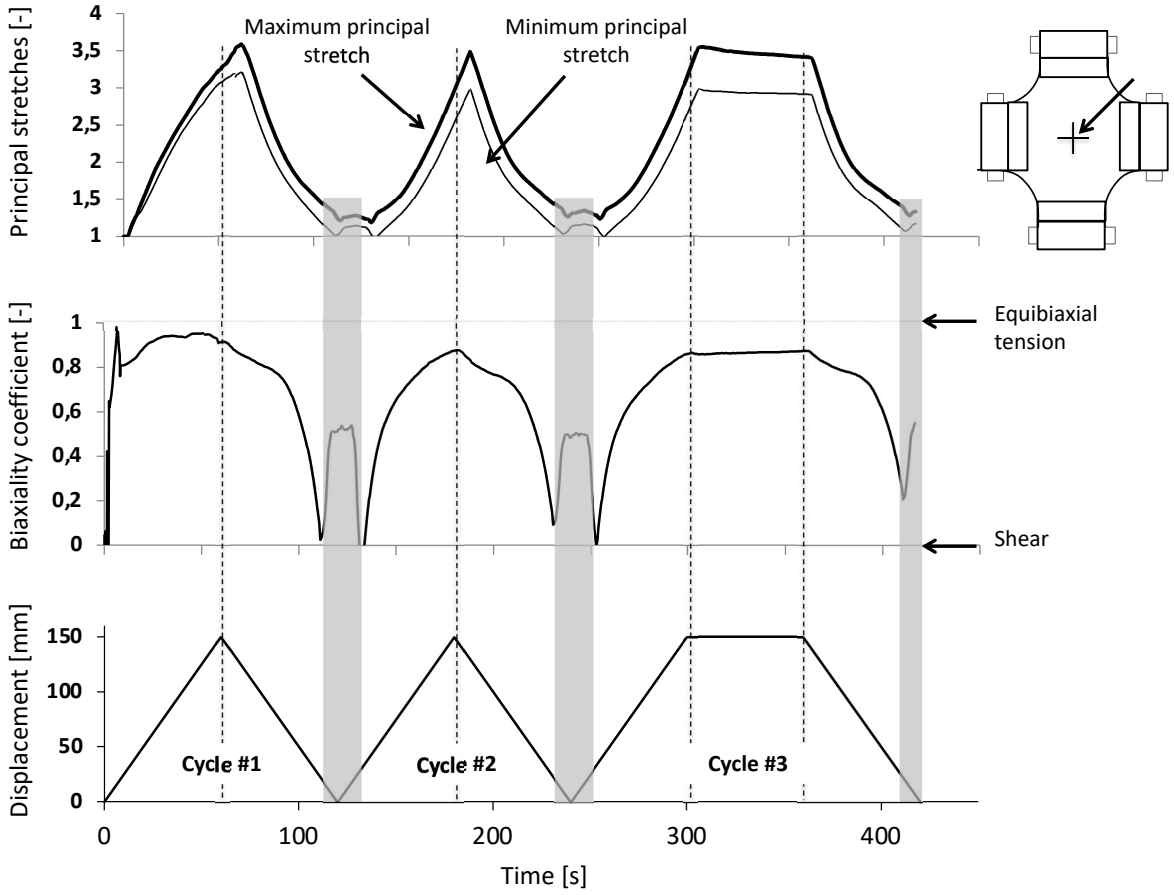

Figure 14: Stretch, biaxiality coefficient and principal stretches in the specimen center versus time

which is the typical signature of SIC (see Box #1). Note that the heat absorbed during the unloading at Cycle #1 is superior to that absorbed at Cycle #2, due to the fact the material is stiffer at the end of the first cycle. The heat absorbed is therefore higher than for the following cycles.

The difference between Cycles #2 and #3 lies in the relaxation phase. When the displacement is kept constant in the branch, a strong heat production is still observed, while the thermo-elastic couplings do not produce heat anymore. This heat production can be due to intrinsic dissipation and/or crystallization. To distinguish the two contributions, the heat absorbed during the unloading of Cycles #2 and #3 is examined. The fact that the heat absorbed during the unloading of Cycle #3 is superior to that absorbed during the

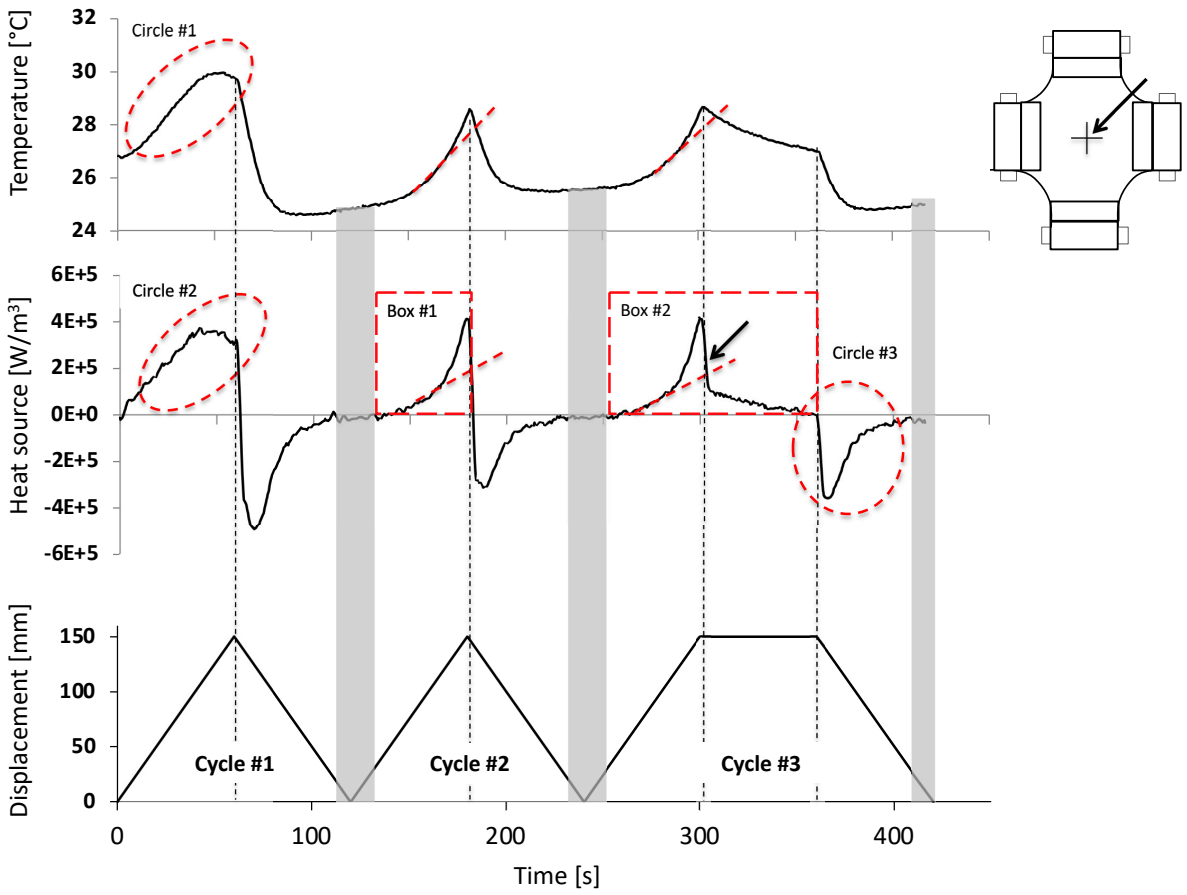

Figure 15: Stretch, temperature and heat source at the specimen center versus time

unloading of Cycle #2 highlights that the main contribution to the heat production due relaxation is SIC. Indeed, if viscosity was the preponderant effect, the heat absorbed during the unloading of Cycles #2 and #3 would have been the same.

6.2.3. Discussion

The previous section has shown that the filled natural rubber considered in this paper crystallizes under biaxial tension. This result is in a good agreement with the one obtained in Beurrot-Borgarino (2012) for a natural rubber vulcanized with 1.2 phr of sulfur and filled with 50 phr of N330 carbon black. In her study, XRD measurements were carried out under uniaxial, biaxial and equibiaxial tension. She found that crystallites are similar in the three

deformation states: the lattice parameters of the crystal unit cell were identical and the size of the crystallites is of the same order of magnitude. Therefore, the present study confirms the first XRD result concerning the effect of multiaxiality on SIC in filled natural rubber. Nevertheless, this is in contradiction with results obtained in unfilled natural rubber by Chen et al. (2019), who found that no crystallization occurs when increasing the biaxiality ratio up to 0.6. Unfortunately in their study, the authors provided neither the precise specimen geometry, nor the boundary conditions applied. The question is therefore whether the presence of fillers alone could explain this difference in results.

In her study, Beurrot-Borgarino (2012) also evaluated the index of crystallinity. Under equibiaxial tension at principal stretches equal to 2.4, a crystallinity index of 1.09% in the plane of tension was found. In this study, an attempt was made to evaluate the crystallinity under biaxial loading. Under uniaxial tension, the crystallinity is expressed by using Eq. 11. An important question is: does the multiaxiality of the strain field have an effect on the fusion enthalpy? According to Beurrot-Borgarino (2012), the size of the crystal unit cell and the size of the crystallites are of the same order of magnitude under uni and biaxial loadings. Thus, it can be assumed here that crystallinity can still be determined from the temperature increases due to crystallization ΔT_{cryst} and the enthalpy of fusion.

Figure 16 provides the heat source obtained during the second loading (red curve) and plotted versus stretch. The heat source due to elastic couplings only (curve in black) is predicted by using Eq. 12 to account for the biaxial strain state. Note that the strong increase in the heat source is obtained at the principal maximum stretch for which $B \geq 0.8$, i.e. a value close to 1 (equibiaxial tension).

The crystallinity evaluated under uniaxial loading is plotted in Fig. 17 versus stretch in order to highlight the effect of the biaxiality ratio. It clearly appears that increasing B from -0.5 to 0.8 led to a decrease in the crystallization onset from 3.2 to 2.6. At the maximum principal stretch of 3.4, the crystallinity reached 1.74%. This seems to be in a good agreement with Beurrot-Borgarino (2012), as the amount of carbon black fillers is lower in the present case.

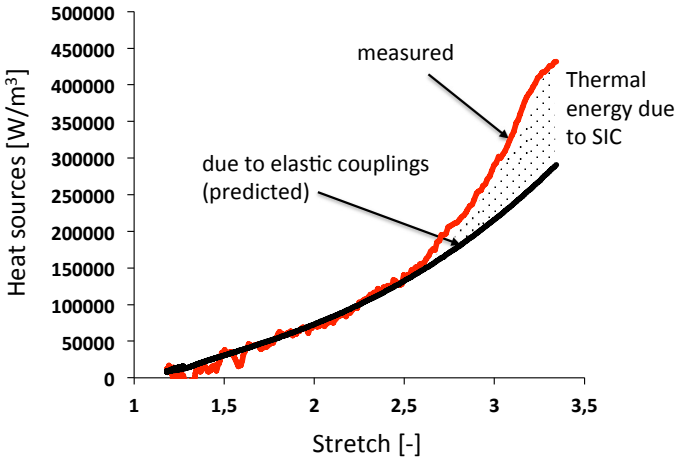

Figure 16: Thermal energy due to crystallization

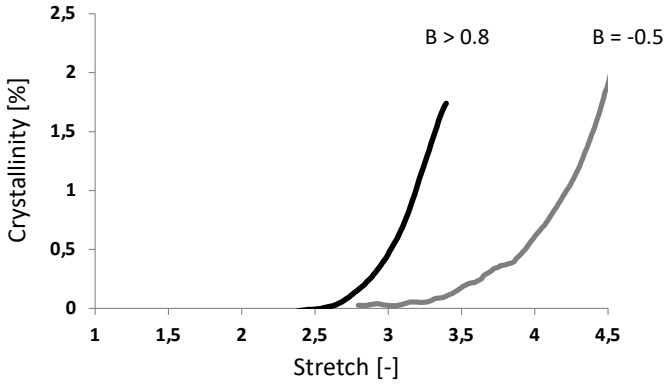

Figure 17: Crystallinity versus stretch and biaxiality coefficient

7. Conclusion

The present study provides the first full thermomechanical and calorimetric characterization of a filled crystallizing natural rubber under uniaxial and biaxial loadings. Under uniaxial loading, sets of several cycles at increasing maximum stretches, with and without accommodation, with and without relaxation have been examined. The corresponding calorimetric response has been determined from the thermal response and the simplified formulation of the heat diffusion equation. A complete energy balance is established for de-

termining the intrinsic dissipation due to viscosity and stress softening. It is shown that the hysteresis loop in the strain-stress relationship mainly corresponds to the energy stored in the material, i.e. the contribution of the viscosity is low. The percentage of the energy stored has been quantified as a function of the applied the maximum stretch. The strain-induced crystallinity and the crystallization onset have also been evaluated from the heat power density response. Biaxial test has then been carried out with a cruciform specimen. The signature of crystallization has been detected in the calorimetric response. Kinematic measurements in the central zone of the specimen have shown that the crystallization onset starts at the principal stretch of 2.6 with a biaxiality coefficient of ca 0.8. This indicates that (i) filled natural rubber crystallizes under high biaxiality coefficient if the principal stretch level applied is high enough (ii) increasing the biaxiality coefficient decreases the crystallization onset (from 3.2 to 2.6 in the present case). This confirms the results by Beurrot-Borgarino (2012) for a natural rubber filled with a larger amount of carbon black fillers. Crystallinity has been evaluated from the calorimetric response by applying the methodology proposed in Le Cam (2018), which was validated with X-ray diffraction measurements in the case of uniaxial loadings. The crystallinity was found to reach 1.74% at the maximum principal stretch of 3.4. These experimental results provide quantitative information of paramount importance for modeling and will be used in the second part of the present paper Khiêm et al. (2021) to propose and validate a physically based model of the complex crystallization behavior of filled natural rubber.

8. Acknowledgements

The authors thank the Contitech AVS France company for providing the material and the specimens. The authors also thank the National Center for Scientific Research (MRCT-CNRS and MI-CNRS), Région Bretagne and Rennes Metropole for supporting this work financially.

References

Anthony, R. L., Caston, R. H., Guth, E., 1942. Equations of state for naturals and synthetic rubber like

materials: unaccelerated natural soft rubber. Journal of Physical Chemistry 46, 826.

Balandraud, X., Le Cam, J. B., 2014. Some specific features and consequences of the thermal response of rubber under cyclic mechanical loading. Archive of Applied Mechanics 84 (6), 773–788.

Benaarbia, A., Chrysochoos, A., Robert, G., 2014. Kinetics of stored and dissipated energies associated with cyclic loadings of dry polyamide 6.6 specimens. Polymer Testing 34, 155–167.

Benaarbia, A., Chrysochoos, A., Robert, G., 2015. Influence of relative humidity and loading frequency on the pa6.6 thermomechanical cyclic behavior: Part ii. energy aspects. Polymer Testing 41, 92 – 98.

Berthel, B., Chrysochoos, A., B.Wattrisse, Galtier, A., 2008. Infrared image processing for the calorimetric analysis of fatigue phenomena. Experimental Mechanics 48, 79–90.

Beurrot-Borgarino, S., 2012. Cristallisation sous contrainte du caoutchouc naturel en fatigue et sous sollicitation multiaxiale. Ph.D. thesis, Ecole Centrale de Nantes (ECN).

Beurrot-Borgarino, S., Huneau, B., Verron, E., Thiaudire, D., Mocuta, C., Zozulya, A., 2014. Characteristics of strain-induced crystallization in natural rubber during fatigue testing: in situ wide-angle x-ray diffraction measurements using synchrotron radiation. Rubber Chemistry and Technology 87 (1), 184–196.
URL https://doi.org/10.5254/rct.13.86977

Bouasse, H., Carrière, Z., 1903. Courbes de traction du caoutchouc vulcanisé. Annales de la Faculté des Sciences de Toulouse 5, 257–283.

Brüning, K., 2014. In-situ structure characterization of elastomers during deformation and fracture. Ph.D. thesis, Technische Universität Dresden, Germany.

Bunn, C., 1942. . Proc. R. Soc. London, Ser. 1 180, 40.

Chen, X., Meng, L., Zhang, W., Ye, K., Xie, C., Wang, D., Chen, W., Nan, M., Wang, S., Li, L., 2019. Frustrating strain-induced crystallization of natural rubber with biaxial stretch. ACS Applied Materials & Interfaces 11 (50), 47535–47544.

Chrysochoos, A., 1985. Energy balance for elastic plastic deformation at finite strain (in french). Journal de Mécanique Appliquée 5, 589–614.

Chrysochoos, A., 1995. Analyse du comportement des matériaux par thermographie infra rouge. In: Colloque Photomécanique. Vol. 95. pp. 201–211.

Chrysochoos, A., Maisonneuve, O., Martin, G., Caumon, H., Chezeau, J. O., 1989. Plastic and dissipated work and stored energy. Nuclear Engineering and Design 114, 323–333.

Demassieux, Q., Berghezan, D., Cantournet, S., Proudhon, H., Creton, C., 2019. Temperature and aging dependence of strain-induced crystallization and cavitation in highly crosslinked and filled natural rubber. Journal of Polymer Science Part B: Polymer Physics 57 (12), 780–793.
URL https://onlinelibrary.wiley.com/doi/abs/10.1002/polb.24832

Farren, W. S., Taylor, G. I., 1925. The heat developed during plastic extension of metals. Proceedings of

the Royal Society of London A: Mathematical, Physical and Engineering Sciences 107 (743), 422–451.

Feuchter, H., 1925. The volume contraction with the formation of anisotropic rubber systems by stretching. Gummi-Ztg 39, 1167–1168.

Harwood, J. A. C., Mullins, L., Payne, A. R., 1965. Stress softening in natural rubber vulcanizates. Part 2. Stress softening effects in pure gum and filler loaded rubbers. Journal of Applied Polymer Science 9, 3011–3021.

Huneau, B., 2011. Strain-induced crystallization of natural rubber: a review of X-ray diffraction investigations. Rubber Chemistry And Technology 84 (3), 425–452.

Immirzi, A., Tedesco, C., Monaco, G., Tonelli, A., 2005. Crystal Structure and Melting Entropy of Natural Rubber. Macromolecules 38, 1223.

Joule, J. P., 1857. On some thermodynamic properties of solids. Phil Mag 4th 14, 227.

Katz, J., 1925. Rntgenspektrographische Untersuchungen am gedehnten Kautschuk und ihre mgliche Bedeutung fr das Problem der Dehnungseigenschaften dieser Substanz. Naturwissenschaften 13, 410.

Khiêm, V. N., Le Cam, J.-B., Charlès, S., Itskov, M., 2021. Thermodynamics of strain-induced crystallization in filled natural rubber under uni- and biaxial loadings. Part II: Physically-based constitutive theory. (submitted).

Lachhab, A., Robin, E., Le Cam, J.-B., Mortier, F., Tirel, Y., Canevet, F., 2018. Energy stored during deformation of crystallizing tpu foams. Strain e12271.

Le Cam, J.-B., 2017. Energy storage due to strain-induced crystallization in natural rubber: the physical origin of the mechanical hysteresis. Polymer 127, 166–173.

Le Cam, J.-B., 2018. Strain-induced crystallization in rubber: A new measurement technique. Strain 54 (1), e12256.

Le Cam, J. B., Albouy, P.-A., Charlès, S., 2020. Comparison between X-ray diffraction and quantitative surface calorimetry based on IR thermography to evaluate strain-induced crystallinity in natural rubber. Submitted to Review of Scientific Instruments.

Legorju-Jago, K., 4-7 septembre 2007. Fatigue life of rubber components: 3d damage evolution from x-ray computed microtomography. In: Constitutive Models for Rubber V - Proceedings of the Second European Conference, Paris, France. pp. 173–177.

Louche, H., 2009. Etudes de certains phénomènes de localisation à partir de champs thermomécaniques. Habilitation thesis, Savoie University.

Loukil, M., Corvec, G., Robin, E., Miroir, M., Le Cam, J.-B., Garnier, P., 2018. Stored energy accompanying cyclic deformation of filled rubber. European Polymer Journal 98, 448 – 455.

Marchal, J., 2006. Cristallisation des caoutchoucs chargés et non chargés sous contrainte : Effet sur les chaînes amorphes. Ph.D. thesis, PhD Thesis, Université Paris XI Orsay, France.

Mason, J., Rosakis, A., Ravichandran, G., 1994. On the strain and strain rate dependence of the fraction of plastic work converted to heat: an experimental study using high speed infrared detectors and the kolsky bar. Mechanics of Materials 17 (2), 135 – 145.
URL http://www.sciencedirect.com/science/article/pii/016766369490054X

Mullins, L., 1948. Effect of stretching on the properties of rubber. Rubber Chemistry and Technology 21, 281–300.

Oliferuk, W., Maj, M., Raniecki, B., 2004. Experimental analysis of energy storage rate components during tensile deformation of polycrystals. Materials Science and Engineering: A 374 (1), 77 – 81.
URL http://www.sciencedirect.com/science/article/pii/S0921509304000735

Rajkumar, G., Squire, J., Arnott, S., 2006. . Macromolecules 39, 7004.

Ramier, J., Chazeau, L., Gauthier, C., Stelandre, L., Guy, L., Peuvrel-Disdier, E., 2007. In situ sals and volume variation measurements during deformation of treated silica sbr. Journal of Materials Science 42, 8130–8138.

Rittel, D., 1999. On the conversion of plastic work to heat during high strain rate deformation of glassy polymers. Mechanics of Materials 31 (2), 131 – 139.
URL http://www.sciencedirect.com/science/article/pii/S0167663698000635

Rittel, D., 2000. An investigation of the heat generated during cyclic loading of two glassy polymers. Part I: Experimental. Mechanics of Materials 32 (3), 131–147.

Rittel, D., Rabin, Y., 2000. An investigation of the heat generated during cyclic loading of two glassy polymers. Part II: Thermal analysis. Mechanics of Materials 32 (3), 149–159.

Roberts, D. E., Mandelkern, L., 1955. Thermodynamics of crystallization in high polymers. natural rubber. Rubber Chemistry and Technology 28 (3), 718–727.

Samaca Martinez, J. R., Le Cam, J.-B., Balandraud, X., Toussaint, E., Caillard, J., 2013a. Mechanisms of deformation in crystallizable natural rubber. part 1: Thermal characterization. Polymer 54, 2717 – 2726.

Samaca Martinez, J. R., Le Cam, J.-B., Balandraud, X., Toussaint, E., Caillard, J., 2013b. Mechanisms of deformation in crystallizable natural rubber. part 2: quantitative calorimetric analysis. Polymer 54, 2727 – 2736.

Samaca Martinez, J. R., Le Cam, J.-B., Balandraud, X., Toussaint, E., Caillard, J., 2014. New elements on mullins effect: a thermomechanical analysis. European Polymer Journal 55, 98–107.

Takahashi, Y., Kumano, T., 2004. Crystal Structure of Natural Rubber. Macromolecules 37, 4860.

Taylor, G. I., Quinney, H., 1934. The latent energy remaining in a metal after cold working. Proceedings of the Royal Society of London A: Mathematical, Physical and Engineering Sciences 143 (849), 307–326.
URL http://rspa.royalsocietypublishing.org/content/143/849/307

Toki, S., Fujimaki, T., Okuyama, M., 2000. Strain-induced crystallization of natural rubber as detected

real-time by wide-angle x-ray diffraction technique. Polymer 41, 5423–5429.

Toki, S., Sics, I., Ran, S., Liu, L., Hsiao, B., Murakami, S., Tosaka, M., Kohjiya, S., Poompradub, S., Ikeda, Y., Tsou, A., 2004. Rubber Chemistry and Technology 42, 956–964.

Trabelsi, S., Albouy, P.-A., Rault, J., 2002. Stress-induced crystallization around a crack tip in natural rubber. Macromolecules 35, 10054–10061.

Trabelsi, S., Albouy, P.-A., Rault, J., 2003. Effective local deformation in stretched filled rubber. Macromolecules 36, 9093–9099.

Vacher, P., Dumoulin, S., Morestin, F., Mguil-Touchal, S., 1999. Bidimensional strain measurement using digital images. Proceedings of the Institution of Mechanical Engineers. Part C: Journal of Mechanical Engineering Science 213.

Zhang, H., Scholz, A. K., Merckel, Y., Brieu, M., Berghezan, D., Kramer, E. J., Creton, C., 2013. Strain induced nanocavitation and crystallization in natural rubber probed by real time small and wide angle x-ray scattering. Journal of Polymer Science Part B: Polymer Physics 51 (15), 1125–1138.
URL https://onlinelibrary.wiley.com/doi/abs/10.1002/polb.23313

V.N.K. and J.-B.L.C.: Conceptualization **J.-B.L.C.:** Methodology, Formal analysis, Resources, Supervision **S.C.:** Investigation, Visualization **J.-B.L.C. and S.C.:** Writing - Original Draft **V.N.K., J.-B.L.C., S.C. and M.I.:** Writing - Review & Editing

Declaration of interests

☒The authors declare that they have no known competing financial interests or personal relationships that could have appeared to influence the work reported in this paper.

☐The authors declare the following financial interests/personal relationships which may be considered as potential competing interests: